

Performance measurement of HARPO: a Time Projection Chamber as a gamma-ray telescope and polarimeter

P. Gros^{*1}, S. Amano², D. Attié³, P. Baron³, D. Baudin³,
 D. Bernard¹, P. Bruel¹, D. Calvet³, P. Colas³, S. Daté⁴,
 A. Delbart³, M. Frotin^{†1}, Y. Geerebaert¹, B. Giebels¹,
 D. Götz⁵, S. Hashimoto², D. Horan¹, T. Kotaka², M. Louzir¹,
 F. Magniette¹, Y. Minamiyama², S. Miyamoto², H. Ohkuma⁴,
 P. Poilleux¹, I. Semeniouk¹, P. Sizun³, A. Takemoto²,
 M. Yamaguchi², R. Yonamine³, and S. Wang^{‡1}

¹LLR, Ecole Polytechnique, CNRS/IN2P3, 91128 Palaiseau,
 France

²LASTI, University of Hyôgo, Japan

³CEA/Irfu Université Paris Saclay, France

⁴JASRI/SPring8, Japan

⁵AIM, CEA/DSM-CNRS-Université Paris Diderot, France

September 2, 2022

Abstract

We analyse the performance of a gas time projection chamber (TPC) as a high-performance gamma-ray telescope and polarimeter in the e^+e^- pair creation regime. We use data collected at a gamma-ray beam of known polarisation. The TPC provides two orthogonal

^{*}philippe.gros at in2p3.fr

[†]Now at GEPI, Observatoire de Paris, CNRS, Univ. Paris Diderot, Place Jules Janssen, 92190 Meudon, France

[‡]Now at INPAC and Department of Physics and Astronomy, Shanghai Jiao Tong University, Shanghai Laboratory for Particle Physics and Cosmology, Shanghai 200240, China

projections (x, z) and (y, z) of the tracks induced by each conversion in the gas volume. We use a simple vertex finder in which vertices and pseudo-tracks exiting from them are identified.

We study the various contributions to the single-photon angular resolution using Monte Carlo simulations and compare them with the experimental data and find that they are in excellent agreement. The distribution of the azimuthal angle of pair conversions shows a bias due to the non-cylindrical-symmetric structure of the detector. This bias would average out for a long duration exposure on a space mission, but for this pencil-beam characterisation we have ensured its accurate simulation by a double systematics control scheme, data taking with the detector rotated at several angles with respect to the beam polarisation direction and systematics control with a non-polarised beam.

We measure, for the first time, the polarisation asymmetry of a linearly polarised gamma-ray beam in the low energy pair creation regime. This sub-GeV energy range is critical for cosmic sources as their spectra are power laws which fall quickly as a function of increasing energy.

This work could pave the way to extending polarised gamma-ray astronomy beyond the MeV energy regime.

1 Introduction

A number of groups are developing pair-conversion detector technologies alternative to the tungsten-converter / thin-sensitive-layer stacks of the COS-B / EGRET / AGILE / *Fermi*-LAT series, to improve the single-photon angular resolution. Presently, observers are almost blind in the 1-100 MeV energy range, mainly due to the degradation of the angular resolution of e^+e^- pair telescopes at low energies: to a large extent, the sensitivity-gap problem is an angular-resolution issue [1].

We have shown [2] that gaseous detectors, such as TPCs (time projection chambers), can enable an improvement of up to one order of magnitude in the single-photon angular resolution (0.5° at 100 MeV) with respect to the *Fermi*-LAT (5° at 100 MeV), a factor of three better than what can be expected for silicon detectors ($1.0\text{-}1.5^\circ$ @ 100 MeV). With such a good angular resolution, and despite a lower sensitive mass, a TPC can close the sensitivity gap at the level of 10^{-6} MeV/cm²s) between 3 and 300 MeV. In addition, the single-track angular resolution is so good that the linear polarisation fraction can be measured.

We first give a brief overview of the experimental configuration, as well as the simulation of the detector and the event reconstruction. We then describe

the analysis procedure, and in particular the event selection. Finally, we show the measured performance of the detector, in terms of angular resolution and polarimetry. The difficulties encountered and the potential for improvement are discussed.

2 Experimental setup

The HARPO (Hermetic ARgon POlarimeter) detector [3] is a demonstrator of the performance of a TPC for measuring polarised γ rays. It was designed for a validation on the ground in a photon beam. The most critical constraints related to space operation were taken into account, such as the reduced number of electronic channels, and long-term gas-quality preservation [4]. It comprises a $(30\text{ cm})^3$ cubic TPC, designed to use a noble gas mixture from 1 to 4 bar. The present work uses an Ar:isobutane (95:5) gas mixture at 2.1 bar. A drift cage provides a 220 V/cm drift field. The electrons produced by the ionisation of the gas drift along the electric field toward the readout plane at a constant velocity $v_{\text{drift}} \approx 3.3\text{ cm}/\mu\text{s}$. The readout plane is equipped with two Gas Electron Multipliers (GEMs) [5] and one Micromesh Gas Structure (Micromegas) [6] to multiply the electrons. The amplified electrons' signal is collected by two sets of perpendicular strips (regular strips in the X -direction, and pads connected together by an underlying strip in the Y -direction. The signals are read out and digitised with a set of AFTER chips [7] and associated Front End Cards (FECs).

The HARPO TPC was set up in the NewSUBARU polarised photon beam line [8] in November 2014. The photon beam is produced by Laser Compton Scattering (LCS) of an optical laser on a high energy (0.6-1.5 GeV) electron beam. Using lasers of various wavelengths and different beam energies [9], 13 photon energies from 1.74 MeV to 74.3 MeV were obtained. In order to mitigate systematic effects due to the geometry of the detector, the detector was rotated around the beam axis to 4 different angular positions (-45, 0, 45 and 90°). Finally, for some configurations (in particular at low energy), data were also taken with randomly polarised photons as a reference.

A trigger system specific to the beam configuration was built using the signals from scintillators, from the micromegas and from the laser. A study of basic event characteristics for various trigger configuration showed that photon signals were recorded with about 50% efficiency, while about 99% of the background was rejected [10].

A specific event reconstruction procedure for pair conversion events was developed [14]. The reconstruction is focused on the local properties of vertices. It does not include any tracking, and does not give any global event

information. We show in the following how this limitation is bypassed using the characteristics of the beam configuration.

3 Data selection

Data were taken with 13 values of photon energy from 1.74 MeV to 74.3 MeV, but not all of them are usable for the analysis. There are two main difficulties:

- Low energy points (below 4 MeV) were obtained using a CO₂ laser without pulsing, and with a high intensity beam. This created a lot of “pile-up” events, where several interactions occurred in the detector within the 15 μ s readout window. Besides, these low energy data are largely dominated by Compton scattering. Data below 4 MeV were therefore discarded.
- The pre-amplifier in the AFTER electronics was found to saturate when a large charge accumulates on a single channel over a few dozen μ s. This induced a loss of signal when tracks were aligned with the drift direction z of the TPC. This signal loss cannot be corrected, and creates a systematic bias in the data. A simple model was used in the simulation which is sufficient to accurately reproduce the systematic bias in the data up to 20 MeV. We do not show polarimetry measurements above this energy.

4 Event selection

The reconstruction [14] relies on local event geometry in 2 dimensions, without tracking. The reconstructed 2D vertices can have one or two associated pseudo-tracks, to accommodate the possibility of overlapping tracks. If both projections of the same vertex have two associated pseudo-tracks, there is a two-fold ambiguity. This ambiguity is resolved by using the ionisation fluctuation along the particle trajectories. The two 2D projections are then combined to obtain a 3D picture.

A reconstructed vertex carries two pieces of information:

- the vertex position \vec{x}_v ;
- the direction \vec{u}_\pm of the associated particles, which are described arbitrarily as electron (“-”) or positron (“+”). The sign of the charge is not necessary for either gamma-ray astronomy or gamma-ray polarimetry.

The opening angle θ_{+-} is defined as:

$$\theta_{+-} = \arccos \vec{u}_+ \cdot \vec{u}_- \quad (1)$$

A vertex can have either one or two associated particles. A vertex with only one associated particle is given an opening angle $\theta_{+-} = 0$.

There are several reconstructed vertices for each event (in particular entry and exit points will be considered as “single particle vertices”). Further topological information is needed to separate real vertices from background. Using the specific configuration of the photon beam, vertices are rejected that are away from the beam or close to the walls of the TPC. Figure 1 show the space distribution of the reconstructed vertices in the TPC. The beam region is visible as a central zone with a higher density. The vertices around are rejected.

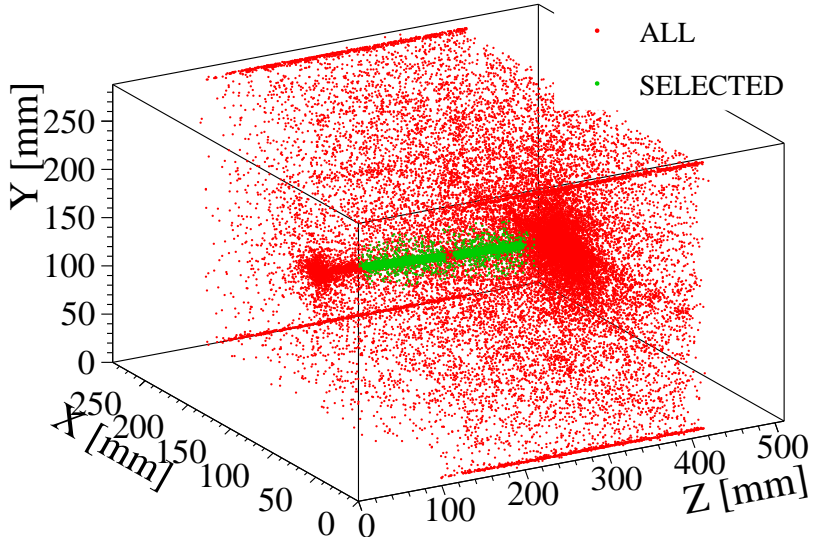


Figure 1: Space distribution of reconstructed vertices in the TPC. The high density region around $z = 100$ mm corresponds to the entry points for conversion events in the material upstream of the gas. The high density region around $z = 400$ mm corresponds to the exit points downstream. The data correspond to 30 minutes of data taking in the 11.8 MeV photon beam. In the middle, the vertices corresponding to interactions of the photon beam with the gas are selected.

Vertices in the beam region have a high probability to have originated from an interaction of a gamma ray with the gas. These interactions are

Compton scattering, pair production in the field of a nucleus (“pair”) or in the field of an electron (“triplet”). They are distinguished by the opening angle θ_{+-} . Figure 2 shows examples of recorded events of each type.

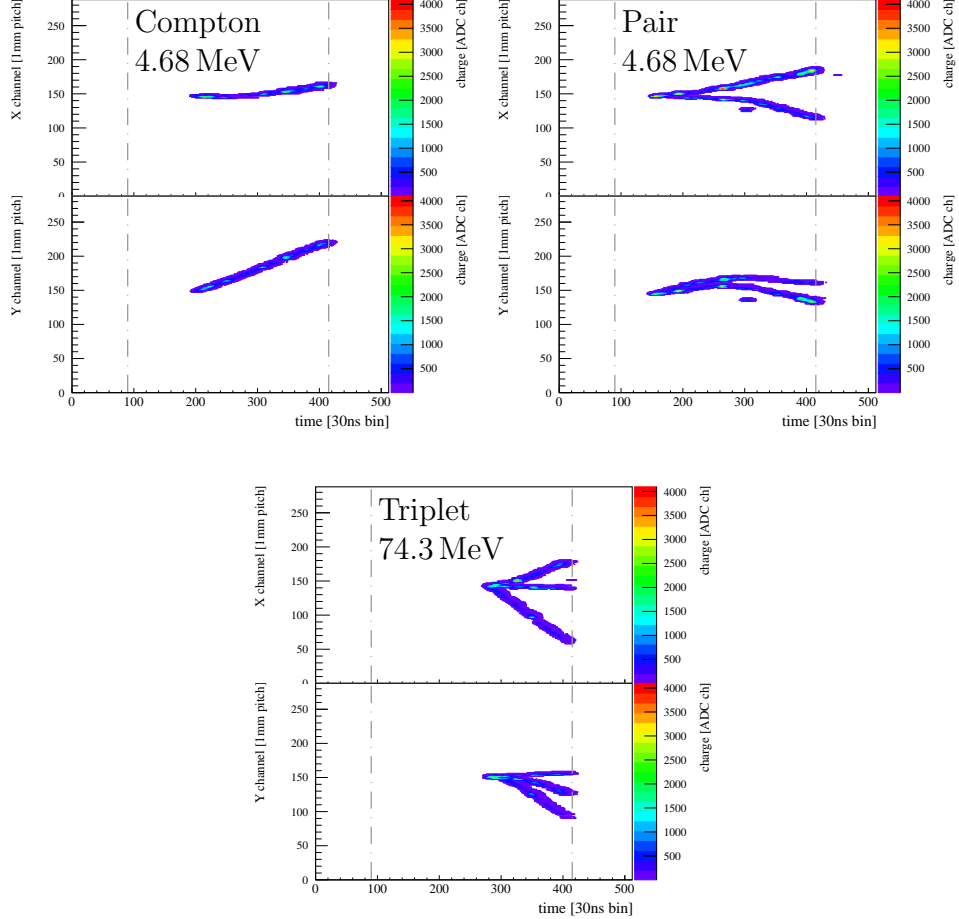


Figure 2: Example of events recorded in the HARPO detector. The three events are identified respectively as Compton scattering, pair conversion and triplet conversion.

For Compton scattering (single track), events can be misreconstructed as pair production (two track) events with small θ_{+-} . Figure 3 shows the distribution of θ_{+-} for 4.68 MeV and 11.8 MeV beam energies, and compares them to simulations, decomposed into Compton scattering, pair and triplet events. The angular distribution is well described by the simulation. The proportion of Compton and pair events is however not correctly reproduced

by the simulation at low energy, suggesting that the trigger efficiency is different for these two categories of events.

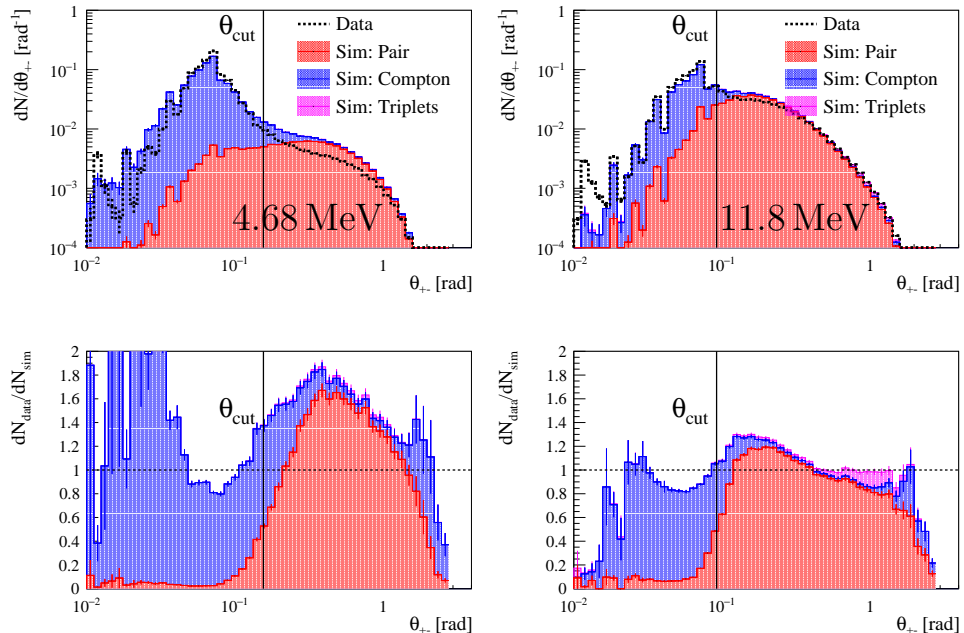


Figure 3: Distribution of the opening angle for 4.68 MeV (left) and 11.8 MeV (right) photon beam energies. The ratio between the data and the simulation is shown in the bottom row. At low energy, the proportion of pair production events seems overestimated in the simulation.

An energy-dependent cut on the opening angle θ_{+-} is used to select the pair events:

$$\theta_{+-} > \left(0.05 + \frac{0.5 \text{ MeV}}{E_\gamma}\right) \text{ rad.} \quad (2)$$

Figure 4 shows the effect of the cut on the opening angle θ_{+-} on the different simulation samples (Compton, pair and triplet), and for the real data. There

is a good agreement between data and simulation. The contamination of the pair production events by Compton scattering events is only of a few percent. Above 40 MeV, the opening angle gets smaller, and it is difficult to distinguish pair events from Compton scattering events.

The selection gives us high purity (over 90%) pair event samples above 4 MeV. At low energy, the stronger cuts applied to remove Compton events reduce the reconstruction efficiency. At high energy, the efficiency is affected by the low opening angles of the conversion events, which cannot be recognised as pairs. In spite of these difficulties, simulations show that the vertices are reconstructed with an efficiency higher than 90% over the whole spectrum presented here.

5 Simulation of the HARPO detector

The cubic geometry of the detector and the configuration of the readout scheme introduce a systematic bias to the polarisation measurement which cannot be addressed analytically. It is therefore necessary to have an accurate simulation of the TPC. We developed a complete simulation to describe the response of the HARPO detector. It contains three main components:

- An event generator describes the conversion of photons in the gas [11, 15]. It provides the energy momentum of the electron-positron pair.
- The interaction of the electron and positron pair with the gas is simulated using Geant4 [16]. It provides the ionisation electrons in the gas volume.
- The processes and geometry of the TPC are described with a custom software [14]. It provides a signal map similar to the real data.

The first two components have been validated in [17] and [15] respectively. The last one was developed specifically for HARPO. The description of the TPC includes electron drift, diffusion and amplification in the gas, the readout space and time response, and the signal digitisation, including known electronics saturation effects.

This simulation was thoroughly validated using a tight selection of cosmic rays. All of the simulation parameters were calibrated against data [18]. Figure 5 shows an example of the comparison between cosmic-ray data and the simulation of the raw-charge read out for each channel and time bin. This distribution is affected by most of the effects mentioned above. There is an excellent agreement between data and simulation.

6 Angular resolution

From a reconstructed vertex, the corresponding photon direction is estimated as $\vec{u}_{\text{pair}} = \vec{u}_+ + \vec{u}_-$. The residual angle θ_{pair} is then:

$$\theta_{\text{pair}} = \arccos(\vec{u}_{\text{pair}} \cdot \vec{u}_\gamma), \quad (3)$$

where \vec{u}_γ is the beam direction. After applying the vertex selection described in Sect. 4, the distribution of the residual angle θ_{pair} was obtained for each configuration of the same energy, polarisation and TPC orientation. Such a distribution for 11.8 MeV photons is shown in Fig. 6.

The angular resolution is dominated by three main effects:

- The momentum of the recoil nucleus is not measured. The corresponding contribution is denoted σ_{recoil} .
- The magnitude of the momentum of the two particles is not measured. The corresponding contribution is denoted σ_p .
- The detector has a finite angular resolution for single charged particles. The corresponding contribution is denoted $\sigma_{\text{det},\gamma}$.

Figure 6 shows the simulated distributions after neglecting each of these effects. The full simulation (“Sim”) gives the resolution $\sigma_{\text{recoil}} \oplus \sigma_p \oplus \sigma_{\text{det},\gamma}$. Using the true track directions, the detector resolution is neglected (“MC truth”), and the resolution is $\sigma_{\text{recoil}} \oplus \sigma_p$. Using the full 4-vector information, the physical limit is reached (“optimal”), and the resolution is σ_{recoil} .

The angular resolution $\sigma_{\theta,68\%}$ is defined as the 68 % containment angle (i.e. the angle such that 68 % of the events have a smaller residual angle). Figure 7 shows the variation of the resolution with energy. The beam data and the detector simulation are consistent. The measured resolution is better by at least a factor 2 than what is obtained by the *Fermi*-LAT, even with a tracking-less reconstruction. A large contribution to the resolution comes from the lack of momentum information.

The three main components of the resolution (σ_{recoil} , σ_p and $\sigma_{\text{det},\gamma}$) are extracted from the simulation. The results are shown in Fig. 8. Below 10 MeV, the main contribution comes from the nucleus recoil. The two other effects give a similar contribution. The beam and detector geometry introduces a systematic bias at low energy (below 5 MeV), so that the final resolution is not the quadratic sum of the components. The two tracks in a pair are correlated, so that the actual resolution for single tracks is not relevant in this context. An effective angular resolution for single tracks can be defined

as $\sigma_{\text{det},e^\pm} = \sigma_{\text{det},\gamma}/\sqrt{2}$. It can be approximated (see Fig. 8) as:

$$\sigma_{\text{det},e^\pm} \approx \left(\frac{p_\pm}{125 \text{ keV}/c} \right)^{-0.64}. \quad (4)$$

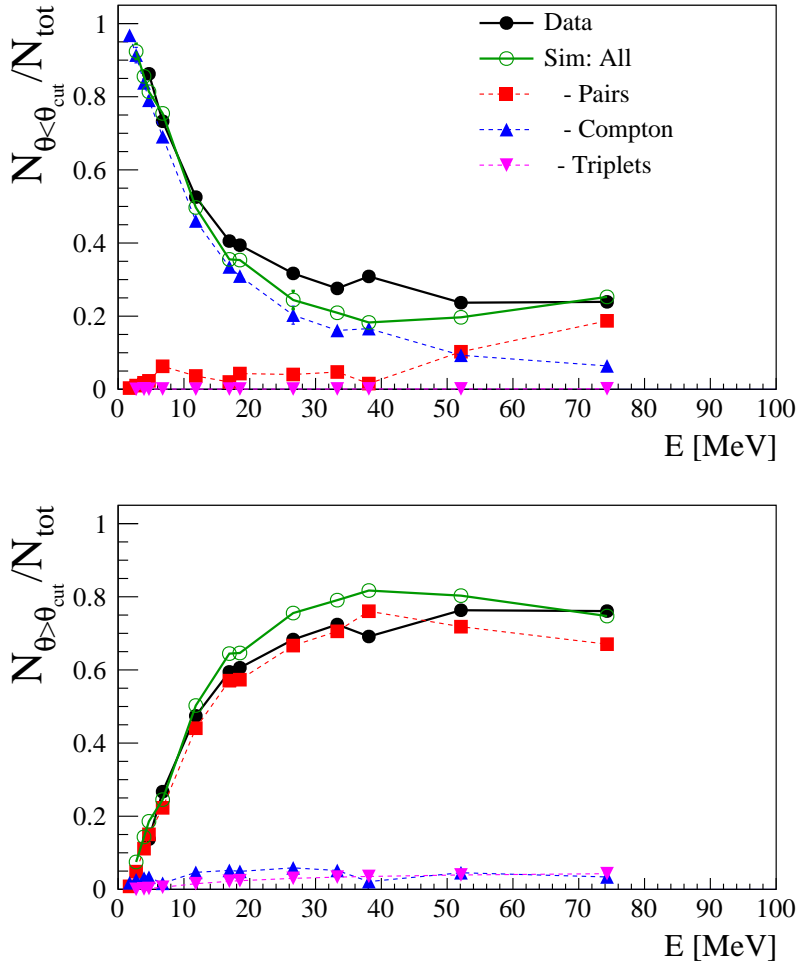


Figure 4: Fraction of the reconstructed vertices that are rejected (top) or selected (bottom) by the cut on the opening angle θ_{+-} . The full lines show the total for data (in black) and simulation (in green). The dashed lines show the contributions of the different processes (Compton, pair and triplets). The data are well reproduced by the simulation, and above 4 MeV more than 90 % of the selected vertices are from pair conversions.

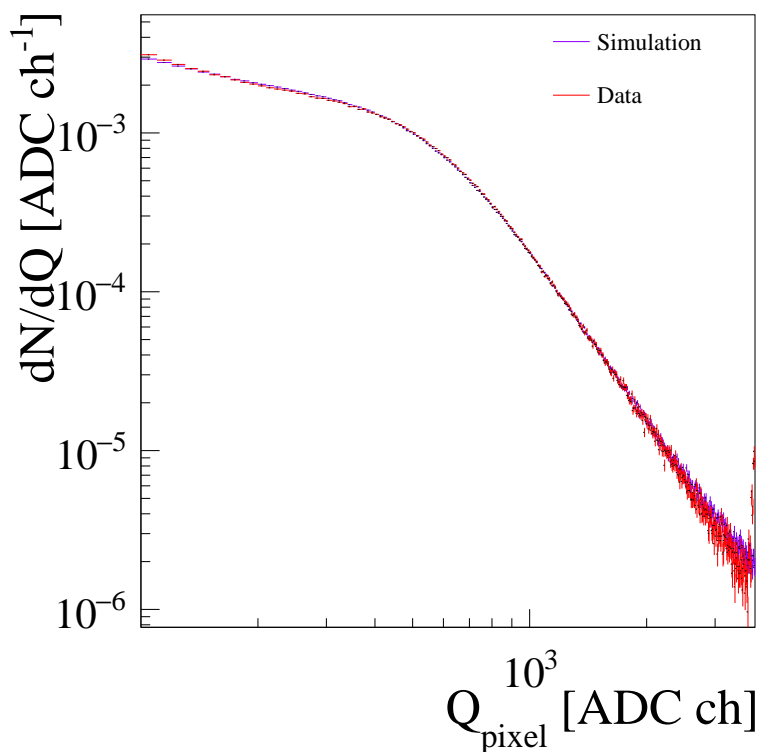


Figure 5: Comparison between data and simulation of the signal amplitude for single pixels. There is excellent agreement between the data and simulation.

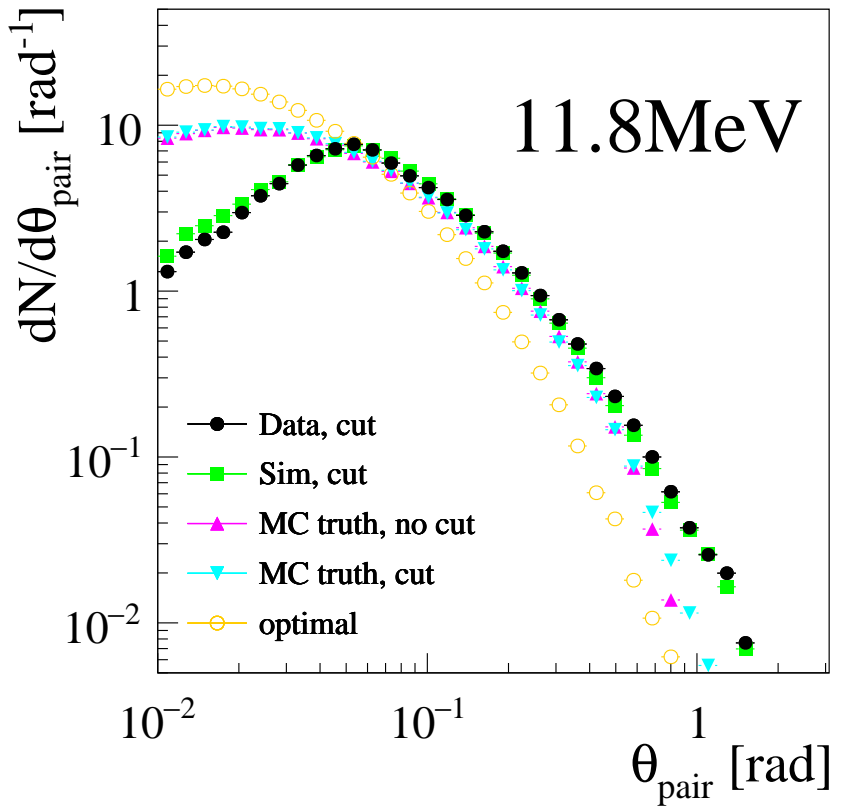


Figure 6: Distribution of the residual angle θ_{pair} for a 11.8 MeV photon beam. Black dots are the beam measurements. Yellow circles show the QED limit, using the full 4-vector information from the Monte-Carlo. The magenta triangles show the residuals using only the track direction from Monte-Carlo (unknown magnitude of the momentum), and the cyan triangles show the effect of the opening angle cut on that distribution. Finally, the green squares show the distribution taking into account the full detector simulation, including contamination from Compton and triplet events. The data are consistent with the full detector simulation.

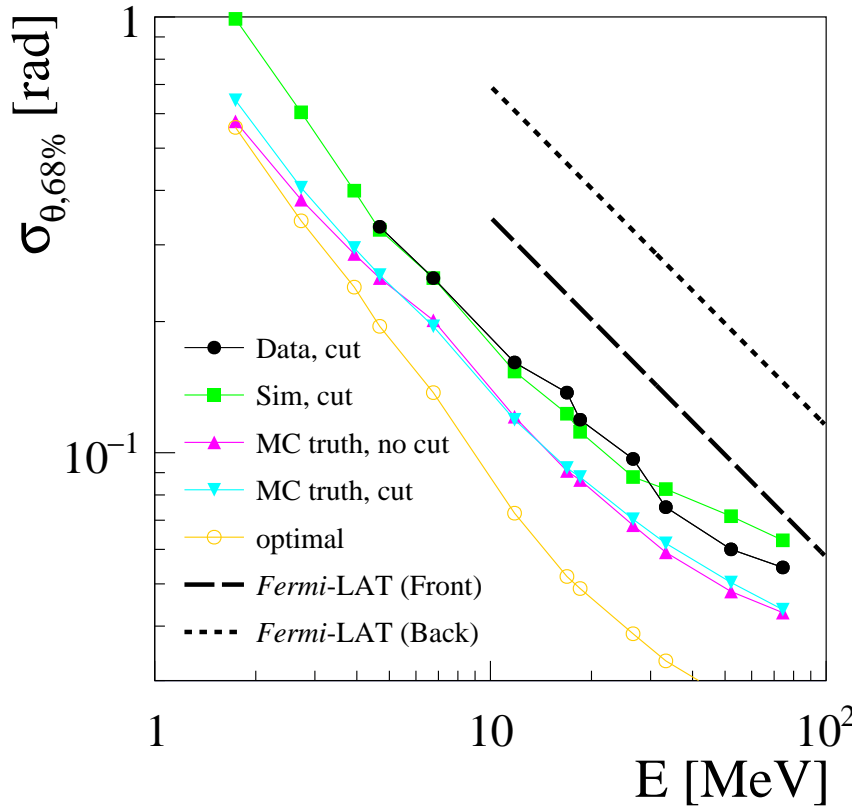


Figure 7: 68% containment angle as a function of the beam energy. The black dots show the measurements in beam. The green squares show the results of a full simulation, including contamination from Compton and triplet events. The magenta triangles show the QED limit in absence of momentum magnitude measurement (ignoring detector effects). The cyan triangles show the effect of the cut (in particular, on the opening angle) on the resolution, ignoring other detector effects. The yellow circles show the QED limit in absence of measurement of the recoiling nucleus. The angular resolution of the *Fermi*-LAT for both front- and back-conversion events is shown for reference as the dashed and dotted lines.

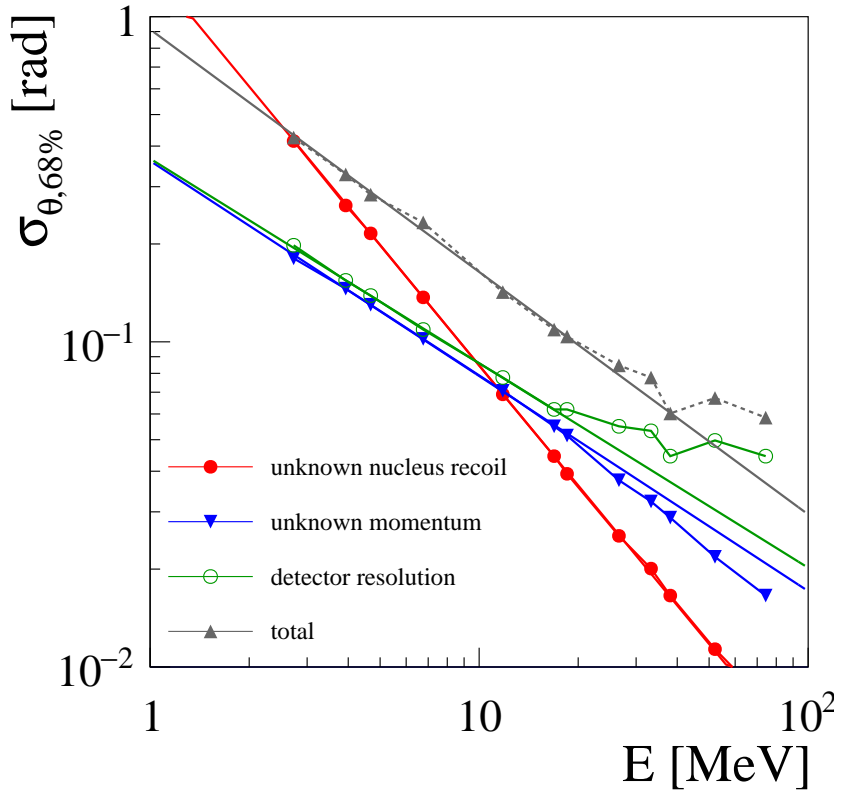


Figure 8: Break down of the contributions to the angular resolution for simulated photons converting with the pair process. Red filled circles show the effect of the unknown recoil momentum. Blue triangles show the effect of the unknown magnitude of the momentum of the two tracks. Green circles show the contribution of the detector effects. This is fitted to a power law with index 0.64. The final resolution of the detector, in gray dashed line, is expected to be the quadratic sum of these components. Each graph is fitted with a power law shown as a straight solid line of the same color. This graph cannot be directly compared to the “Sim, cut” graph in Fig. 7, which also includes the contribution of Compton and triplet events.

7 Polarimetry

Following [12], an optimal estimate of the polarisation asymmetry is given by the distribution of $\phi_{+-} = (\phi_+ + \phi_-)/2$, where ϕ_{\pm} is the azimuthal angle of the particle with regard to the beam axis:

$$\phi_{\pm} = \arctan \frac{u_{\pm}^X}{u_{\pm}^Y}, \quad (5)$$

where X, Y are the coordinates in a plane perpendicular to the beam direction, and X is the direction of the beam polarisation.

The distribution of ϕ_{+-} is obtained for each configuration of same energy, polarisation and TPC orientation. Figure 9 shows an example of the distributions for 11.8 MeV photons in each of the configurations. There are large systematic effects due to the cubic geometry of the detector and the fixed direction of the photons.

The geometry effects are cancelled out by taking the ratio of the polarised and unpolarised beam data. Figure 10 shows the result for the four different orientations of the detector around the beam axis. The systematic bias is further reduced by combining the data with different orientations, resulting in Fig 11. Since the unpolarised data are not available for every configuration, the simulation is used to correct the systematic bias. Figure 11, bottom, shows the ratio of real polarised beam data with a simulated unpolarised beam. In each case, the distribution is fitted with the expected function $1 + A \cos 2(\phi - \phi_0)$, where A is the measured polarisation asymmetry.

The above results are strongly influenced by the fixed configuration of the photon beam. In the case of a space telescope, the systematic bias would be very different. Figure 12 shows the azimuthal angle distribution for simulated isotropic 11.8 MeV photons, converting uniformly inside the detector. This represents a simple model for a long duration exposure in a space mission. The reconstructed azimuthal angle is uniform for an unpolarised source, and shows the expected modulation when the photons are polarised. In that case, no correction is applied. The measured amplitude A of the polarisation asymmetry in this case cannot be directly compared with what is measured in beam data. The amplitude A depends on the fiducial cuts chosen, because the angular resolution depends on the length of the particle trajectories inside the detector. An optimisation of these cuts is necessary to assess the polarimetry potential in such a configuration.

Figure 13 shows the measured polarisation asymmetry A obtained in each of the following cases:

- ratio of polarised data over unpolarised data;

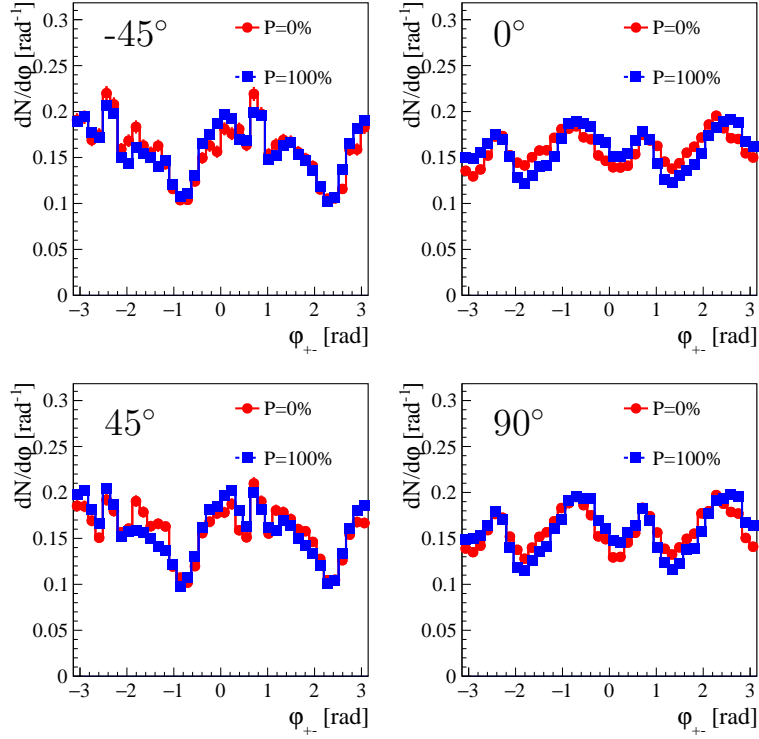


Figure 9: Distribution of ϕ_{+-} for 11.8 MeV photons, for four orientations of the HARPO TPC (-45°, 0°, 45° and 90°) around the beam axis. Data from polarised and unpolarised beam are shown with the blue squares and the red dots respectively.

- ratio of polarised simulation over unpolarised simulation;
- ratio of polarised data over unpolarised simulation;
- ratio of polarised simulation over unpolarised data (as a validation of the method).

The optimal value of the polarisation asymmetry A from QED is calculated using an exact event generator [12]. In addition to the full simulation represented in Fig. 11, we estimate the contribution of the single-track angular resolution, alone, to the dilution of the polarisation asymmetry. The finite resolution on the azimuthal angle σ_ϕ dilutes this asymmetry by a factor $D = e^{-2\sigma_\phi^2}$. Approximating the opening angle of the pair by its most probable

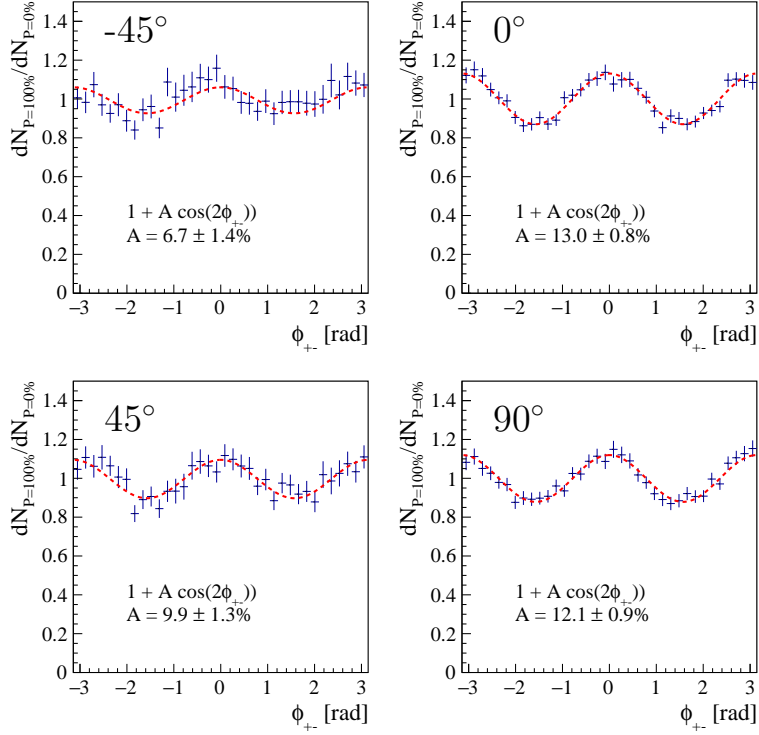


Figure 10: Ratio of the azimuthal angle distributions for polarised ($P=100\%$) and unpolarised ($P=0\%$) 11.8 MeV photons. The systematic bias is cancelled by dividing the azimuthal angle distribution for polarised photons by the distribution for unpolarised photons (experimental data). Four orientations of the detector around the beam axis (-45° , 0° , 45° , and 90°) were used.

value $\hat{\theta}_{+-} \approx E_0/E$ (with $E_0 = 1.6$ MeV) [13] gives:

$$\sigma_\phi \approx \frac{\sigma_{\theta,e^+} \oplus \sigma_{\theta,e^+}}{\hat{\theta}_{+-}} = \frac{\sqrt{2}\sigma_{\text{det},e^\pm}}{\hat{\theta}_{+-}} \quad (6)$$

where $\sigma_{\text{det},e^\pm}$ is the effective angular resolution of the detector (Eq. 4). This gives an expected value for the measured polarisation asymmetry, which is shown as the green dashed line and the open stars in Fig. 13. The measured polarisation asymmetry is found to be consistent with the QED limit, taking into account the detector's angular resolution.

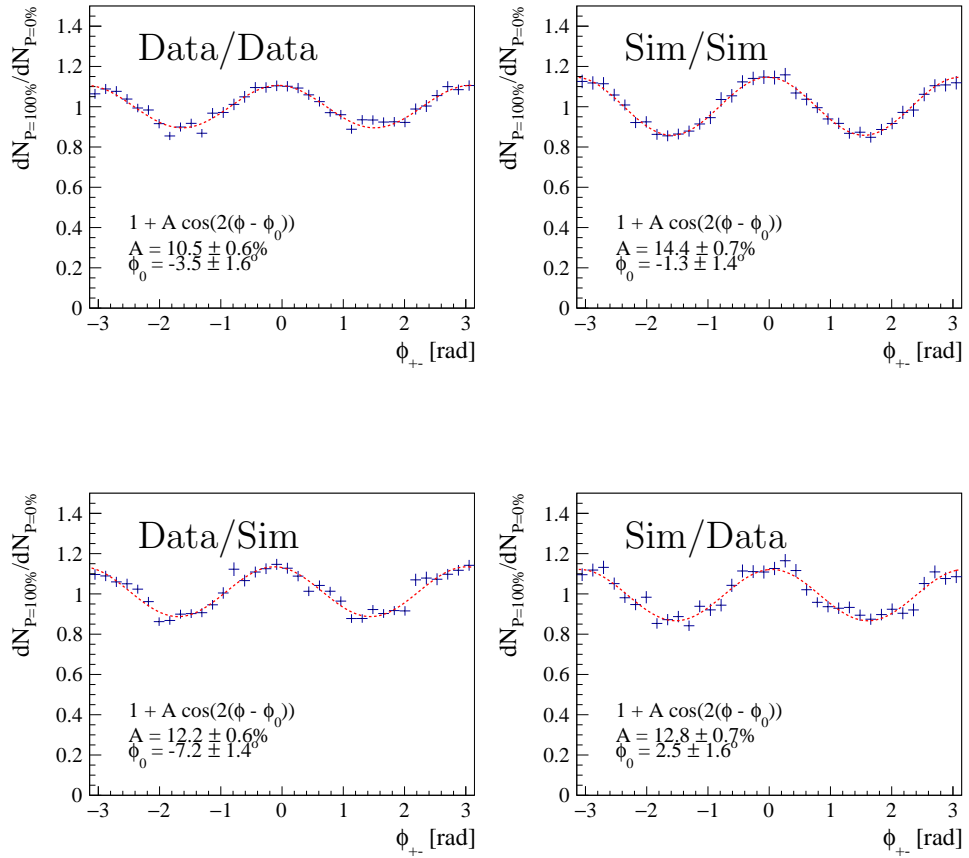


Figure 11: Ratio of the azimuthal angle distributions for polarised (P=100%) and unpolarised (P=0%) 11.8 MeV photons. Top left: ratio of polarised data over unpolarised data. Top right: ratio of polarised MC over unpolarised MC. Bottom left: ratio of polarised data over polarised MC. Bottom right: ratio of polarised MC over unpolarised data.

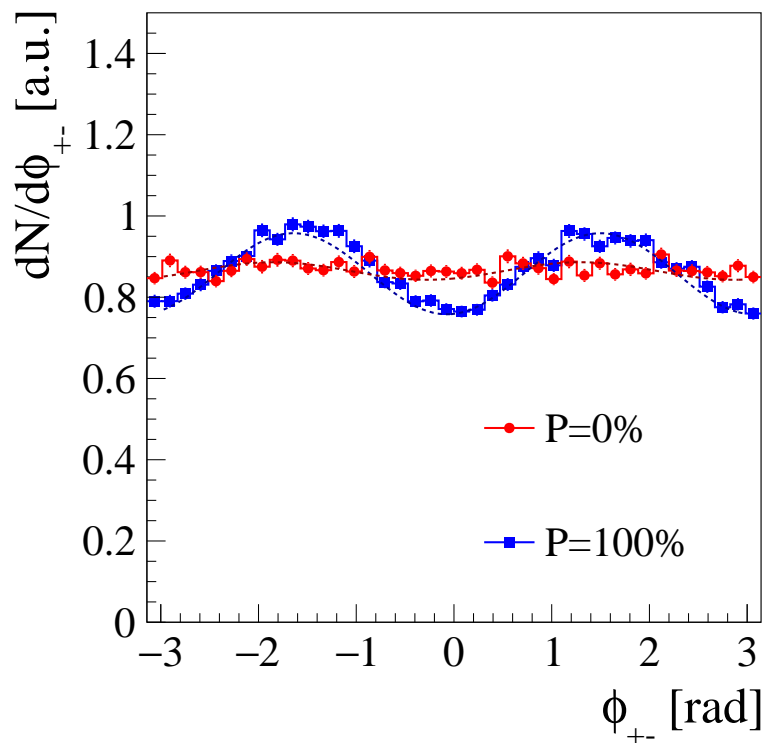


Figure 12: Simulated distribution of ϕ_{+-} for 11.8 MeV photons, for isotropic photons. The interaction points are uniformly distributed in the detector. Data from a polarised and an unpolarised source are shown with the blue squares and the red dots respectively.

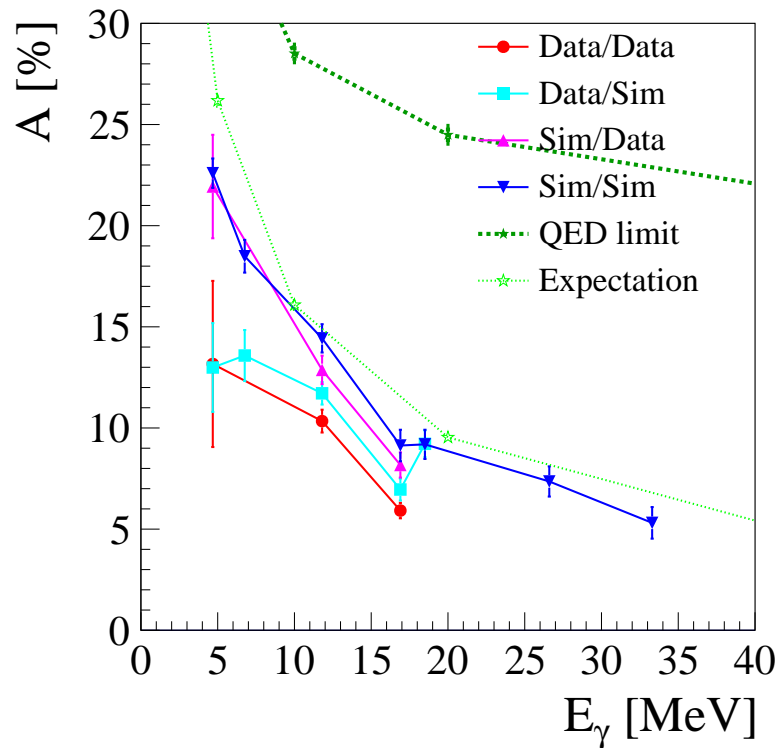


Figure 13: Measured polarisation asymmetry as a function of the photon energy, using the ratio of ϕ_{+-} distributions for polarised and unpolarised photons. The QED limit from the pair-conversion kinematics is shown as a thick green dashed line, with full stars. The light green dashed line with open stars is this same limit, corrected to take into account the angular resolution for the tracks.

8 Discussion

The data shown here were obtained in a photon beam with high flux, which is not representative of the situation for a telescope for cosmic gamma rays. This high event rate created extra difficulties related, in particular, to the saturation of the readout electronics. The event reconstruction could not be completed and optimised due to the limited resources of the project. The results shown here should therefore be seen as a lower limit to the capabilities of the detector.

The detector performance can be further improved in several ways:

- reduction of the electronics saturation, by using a more adapted dynamic range;
- improvement of the vertexing algorithm, using more adapted peak finding method;
- introduction of a tracking algorithm, for event categorisation and possible resolution improvement;
- introduction of a track-momentum estimation using multiple scattering[19].

All of these methods should improve the resolution of the detector, without requiring any hardware modifications.

9 Conclusion

We have built a TPC for gamma-ray detection and polarimetry and we have successfully operated it in a polarised photon beam between 1.74 MeV and 74 MeV. We have developed a simple but effective event reconstruction for pair production, and a detailed and accurate detector simulation. Measurements of the angular resolution are consistent with simulations and offer an improvement of at least a factor 2 over the *Fermi*-LAT. This resolution can be further improved with simple modifications of the hardware and software. We show the first measurements of the polarisation of pair-production photons below 50 MeV.

The behaviour of the detector is very well reproduced by the simulation. We can now confidently use the simulation to investigate improvements, and to estimate the performance of such a detector for cosmic gamma-ray measurement in the high atmosphere or in space.

This work was funded by the French National Research Agency (ANR-13-BS05-0002) and was performed by using NewSUBARU-GACKO (Gamma Collaboration Hutch of Konan University).

References

- [1] Julie McEnery, “Fermi-LAT below 100 MeV”, “e-ASTROGAM workshop: the extreme Universe”, Padova Feb-March 2017
- [2] D. Bernard, “TPC in gamma-ray astronomy above pair-creation threshold,” *Nucl. Instrum. Meth. A*, vol. 701, p. 225, 2013.
- [3] P. Gros *et al.*, “HARPO - TPC for High Energy Astrophysics and Polarimetry from the MeV to the GeV,” *Proceedings of Science*, vol. TIPP2014, p. 133, 2014.
- [4] M. Frotin *et al.*, arXiv:1512.03248 [physics.ins-det].
- [5] F. Sauli, *GEM: A new concept for electron amplification in gas detectors*, Nucl. Instrum. Meth. A **386**, 531 (1997).
- [6] Y. Giomataris, P. Reboursard, J. P. Robert and G. Charpak, *MICROMEGAS: A high-granularity position-sensitive gaseous detector for high particle-flux environments*, Nucl. Instrum. Meth. A **376**, 29 (1996).
- [7] D. Calvet, “A Versatile Readout System for Small to Medium Scale Gaseous and Silicon Detectors,” *IEEE Trans. Nucl. Sci.*, vol. 61, no. 1, pp. 675–682, 2014.
- [8] K. Horikawa, S. Miyamoto, S. Amano, and T. Mochizuki, “Measurements for the energy and flux of laser Compton scattering γ -ray photons generated in an electron storage ring: NewSUBARU,” *Nuclear Instruments and Methods in Physics Research Section A: Accelerators, Spectrometers, Detectors and Associated Equipment*, vol. 618, no. 1-3, pp. 209 – 215, 2010.
- [9] S. Wang *et al.*, “HARPO: a TPC concept for γ -ray polarimetry with high angular resolution in the MeV-GeV range,” *J. Phys. Conf. Ser.*, vol. 650, p. 012016, 2015.
- [10] S. Wang, “Etude d’une TPC, cible active pour la polarimétrie et l’astronomie gamma par création de paire dans HARPO”, PhD thesis, Ecole Polytechnique, 2015. *in French*
- [11] D. Bernard, “Polarimetry of cosmic gamma-ray sources above e^+e^- pair creation threshold,” *Nucl. Instrum. Meth. A*, vol. 729, p. 765, 2013.

- [12] “ γ -ray polarimetry with conversions to e^+e^- pairs: polarisation asymmetry and the way to measure it”, P. Gros and D. Bernard, Astroparticle Physics 88 (2017) 30, doi 10.1016/j.astropartphys.2016.12.006, arXiv:1611.05179 [astro-ph.IM].
- [13] “Opening Angles of Electron-Positron Pairs”, Haakon Olsen, Phys. Rev. 131, 406 - 415 (1963).
- [14] “Measurement of polarisation asymmetry for gamma rays between 1.7 to 74 MeV with the HARPO TPC”, P. Gros *et al.*, SPIE2016, 9905-95.
- [15] P. Gros and D. Bernard, Astropart. Phys. **88** (2017) 60 doi:10.1016/j.astropartphys.2017.01.002 [arXiv:1612.06239 [astro-ph.IM]].
- [16] J. Allison *et al.*, “Geant4 developments and applications,” *IEEE Transactions on Nuclear Science*, vol. 53, pp. 270–278, Feb 2006.
- [17] K. Amako *et al.*, IEEE Trans. Nucl. Sci. **52** (2005) 910. doi:10.1109/TNS.2005.852691
- [18] “A TPC as high performance gamma-ray telescope and polarimeter: polarisation measurement in a beam between 1.7 and 74MeV with HARPO”, P. Gros *et al.*, proceedings to be published in *Journal of Physics: Conference Series (JPICS)*.
- [19] *M. Frosini and D. Bernard, arXiv:1706.05863 [physics.data-an]*.